Materials and Design 39 (2012) 151–161

Contents lists available at SciVerse ScienceDirect

Materials and Design

journal homepage: www.elsevier.com/locate/matdes

Study on laser beam welding/superplastic forming technology of multi-sheet cylinder sandwich structure for Inconel718 superalloy with ultra-fine grains

F.S. Qu [a,*], Z. Lu [b], F. Xing [a], K.F. Zhang [b]

[a] Chongqing University, College of Material Science and Engineering, Chongqing 400030, China
[b] Harbin Institute of Technology, School of Materials Science and Engineering, Harbin 150001, China

ARTICLE INFO

Article history:
Received 29 September 2011
Accepted 2 February 2012
Available online 13 February 2012

Keywords:
C. Forming
B. Sandwich structures
D. Welding

ABSTRACT

Multi-sheet cylinder sandwich structure of Inconel718 superalloy will be widely used in aerospace as heat resisting and heat shielding structure due to its lightweight, high strength and stiffness. Superplasticity of Inconel718 superalloy was investigated. Under $T = 950$ °C and initial strain rate with $\dot{\varepsilon} = 1.6 \times 10^{-4}$ s^{-1}, the elongation of Inconel718 superalloy is 483.6%. The perfect superplastic forming temperature for Inconel718 superalloy is at 950 °C. The laser penetration welding parameters are as follows: power 1200 W, welding speed 1200 mm/min, defocusing amount −1 mm, shield gas flow 0.6 L/min, and the parameters for superplastic forming are as follows: temperature $T_f = 950$ °C, pressure $P_f = 4.2$ MPa, time $t_f = 130$ min. The multi-sheet cylinder sandwich structure manufactured by laser beam welding/superplastic forming (LBW/SPF) technology has good shape, uniform wall thickness distribution, high symmetry in internal structure. Laves phase, harmful to the materials, translates to the δ phase which will help improve the performance of the material after SPF process. The hardness of laser welding joints is improved from 331.63 HV to 391.74 HV after the SPF process. The tensile strength of base material of multi-sheet cylinder sandwich structure has been increased about 261 MPa after the SPF process.

1. Introduction

Inconel718 is a nickel-based superalloy which is strengthened by a bcc Ni_3Nb (γ'') and fcc Ni_3 (Al, Ti, Nb) (γ') [1]. It is widely used for aviation, aerospace, petroleum, chemicals, energy and other fields [2–4]. It is well known that Inconel718 superalloy with ultra-fine grain possesses superplasticity and there have been many documentations on the complex-shaped components processed by superplastic forming [5–7]. Multi-sheet cylinder sandwich structures of Inconel718 superalloy are widely applied in aerospace as heat resisting and heat shielding structure due to its lightweight, high strength and stiffness, and it can be used for low-cost, lightweight rocket engine, such as engine manifold or similar parts. Generally the multi-sheet sandwich structures are manufactured by superplastic forming/diffusion bonding (SPF/DB) technology. But the creep strength of Inconel718 superalloy is so high that this makes its diffusion bonding connection pressure and temperatures high. Its diffusion bonding temperature is 1050 °C, connection time and pressure are 45 min and 20 MPa, respectively [8]. But under this condition of diffusion bonding, Inconel718 superalloy grains growing severely results in the loss of superplasticity of Inconel718 because δ precipitated phase dissolving completely into the matrix leads to that it can not pin down the grain boundary to control grain size [9]. In addition, the low strength of diffusion bonding joints of Inconel718 superalloy can not meet the requirement of multi-sheet sandwich structure forming [8]. Additionally, the special geometry of multi-sheet cylinder sandwich structure is improperly fabricated by SPF/DB technology. In conclusion, SPF/DB technology is improper to manufacture multi-sheet cylinder sandwich structure of Inconel718 superalloy. Laser beam welding as a joining method is being rapidly applied in various industries, from automotive to aerospace, due to its advantages over conventional welding methods such as high speed, low distortion, low heat input, and narrow width of the fusion zone and the heat affected zone (HAZ) [10–13]. In recent years, laser beam welding/superplastic forming/diffusion bonding (LBW/SPF/DB) technology which was presented as extension and supplement of SPF/DB technology has fairish effect on heavy gauge Ti-alloy multi-sheet sandwich structures [14]. In this paper, laser beam welding/superplastic forming (LBW/SPF) technology will be applied to fabricate multi-sheet cylinder sandwich structure with complicated interior structure of Inconel718 superalloy with ultra-fine grain. For verifying the applicability of LBW/SPF technology for multi-sheet cylinder sandwich structure of Inconel718 superalloy with ultra-fine grain, LBW/SPF technology and material science will be integrated using the scheme: LBW/SPF techniques to fabricate multi-sheet cylinder sandwich

* Corresponding author. Tel.: +86 23 6510 3065; fax: +86 23 6511 1493.
E-mail address: qufengsheng@cqu.edu.cn (F.S. Qu).

0261-3069/$ - see front matter © 2012 Elsevier Ltd. All rights reserved.
doi:10.1016/j.matdes.2012.02.002

structure→microstructures and mechanical properties of multi-sheet cylinder sandwich structure, to validate the applicability of LBW/SPF technology for multi-sheet cylinder sandwich structure of Inconel718 superalloy with ultra-fine grain.

2. Experimental procedure

Test material is Inconel718 superalloy sheet with ultra-fine grain, processing for the ultra-fine grains: 1050 °C for 0.5 h with successive water quenching, 50% cold rolling + 890 °C × 10 h δ-phase precipitation treatment + 30% cold rolling + 950 °C × 3 h recrystallization annealing. The grain size is ASTM13-14 [15]. Its chemical composition is shown in Table 1. The sizes of each sheet for multi-sheet cylinder sandwich structure are: the inner canister 703.42 mm × 240.00 mm × 1.30 mm; core canister 710.10 mm × 150.00 mm × 1.10 mm; the outer canister 718.48 mm × 240.00 mm × 1.30 mm.

Superplastic tensile of Inconel718 superalloy with ultra-fine grain was carried out in Instron5500R universal testing machine. It is heated by electrical resistance furnace. Temperature is controlled in three zones and error is less than ±0.1 °C. The 'm' value of inconel718 superalloy with ultra-fine grain was measured by Gleeble-1500 thermal simulation testing machine. The value of strain rate sensitivity was measured by the method of Backfen.

The laser welding for multi-sheet cylinder sandwich structure was carried out in the cross-flow CO_2 continuous laser generator (DC030-type made in German ROFIN Company). Shear strengths of laser penetration welding joints were tested in Instron5569 electronic universal material testing machine.

The multi-sheet cylinder sandwich structure after laser welding was made into a gas pack by GTAW. The workpiece and die was put into 1500 kN superplastic forming machine, heated to 950 °C and remained for 30 min to make them fully hot. Then superplastic forming was performed.

The microstructures of laser welding joint and the base material were investigated with the optical and scanning electron microscopy (SEM). Specimens for optical and scanning electron microscopy were prepared as per standard metallographic practices. Polished specimens were electrolytically etched with an aqueous solution of 50% HCl at 2–3 V for about 10 s. Optical microstructures were observed by OLYMPNS-GX51. SEM was carried out in the FEI QAUANTA 2000 scanning electron microscope. Element concentration of precipitated phase and dendritics in the weld fusion was estimated by EDAX spot analysis. Microhardness measurements for weld joint and base material were performed using a Vicker microhardness tester at a load of 100 g with 15 s. The tensile strength of base material in room temperature was measured in Instron5569 electronic universal material testing machine.

3. Results and discussion

3.1. Superplasticity of Inconel718 superalloy with ultra-fine grain

In order to make multi-sheet cylinder sandwich structure form favorably, superplasticity of Inconel718 sheet with ultra-fine grains is required to study in depth. Constitution diagram of Inconel718 superalloy is shown in Fig. 1. As can be seen from Fig. 1, the grain level is ASTM13-14 [15], and it is fit for superplastic forming. The

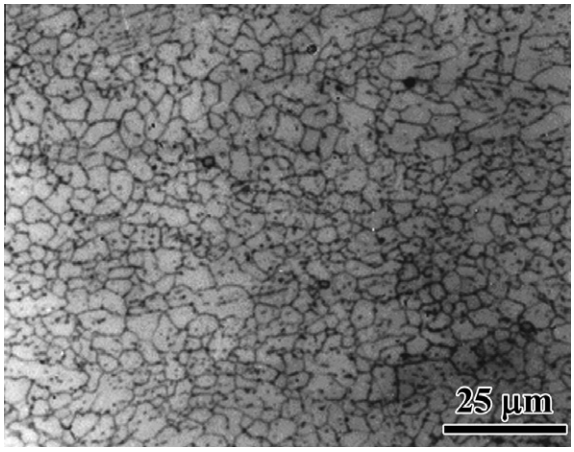

Fig. 1. Microstructure of Inconel718 superalloy with ultra-fine grain.

effect of the temperature on the elongation under the same initial strain rate is shown in Fig. 2. The tensile specimens' photo is shown in Fig. 3. When the initial strain rate ($\dot{\varepsilon}$) is at $3.1 \times 10^{-4}\ s^{-1}$, the elongations of Inconel718 are all greater than 300% at 920–965 °C. The alloy exhibits favorable superplasticity behaviors. The best elongation is 440.3% at 950 °C. When the tensile temperature reaches or exceeds 980 °C in this experiment, the elongation of Inconel718 superalloys with ultra-fine grain obviously declines. The reason is that when the deformation temperature exceeds 970 °C, it leads to the grains grow rapidly during the deformation process that δ precipitated phase dissolving into γ phase results in that it can not pin down the grain boundary to control grain size [16].

The variation behavior of the initial flow stress is shown in Fig. 4. From Fig. 4, it can be seen that the initial flow stresses of Inconel718 superalloy submit monotone downtrend when deformation temperature increases monotonously. At 950–995 °C, the low initial flow stresses are fit for superplastic puff forming. However, when the temperature reaches or exceeds 970 °C, δ phase starting to dissolve into γ phase leads to grain growth [16], which reduces its superplastcity and makes subsequent flow stress increase. In the process of forming multi-sheet cylinder sandwich structure, high elongation and low flow stress are required in order to ensure internal structure fully formed. So the ideal superplastic forming temperature is at 950–965 °C. In addition, the difference of flow stress in the range of experimental temperature is 20.5 MPa, changing by only 30%.

Superpasticity elongation variation at the 950 °C under the different initial strain rate is shown in Fig. 5. When the initial strain rate changes in the range of $1.6 \times 10^{-4}\ s^{-1}$–$2.0 \times 10^{-3}\ s^{-1}$, the elongations of Inconel718 superalloy are all greater than 250%, which shows good superplasticity performance. At the strain rate of $1.6 \times 10^{-4}\ s^{-1}$, the best elongation of 483.6% can be obtained. The photo of comparison sample is shown in Fig. 6. When the initial strain rate changes in the range of $1.6 \times 10^{-4}\ s^{-1}$–$2.0 \times 10^{-3}\ s^{-1}$, the elongation of Inconel718 superalloy decreases with strain rate increasing.

The initial flow stress of Inconel718 superalloy under the same deformation conditions is shown in Fig. 7. The initial flow stresses in company with the initial strain rate increasing act like the

Table 1
Chemical composition of Inconel718 alloy (wt%).

C	Si	Mn	Ni	Cr	Fe	Co	Ti	Al	Mo	Nb	S	P	Mg	Cu	B
0.067	0.08	0.03	53.32	19.26	16.42	0.05	1.13	0.55	3.26	5.73	0.005	0.008	<0.01	0.072	0.006

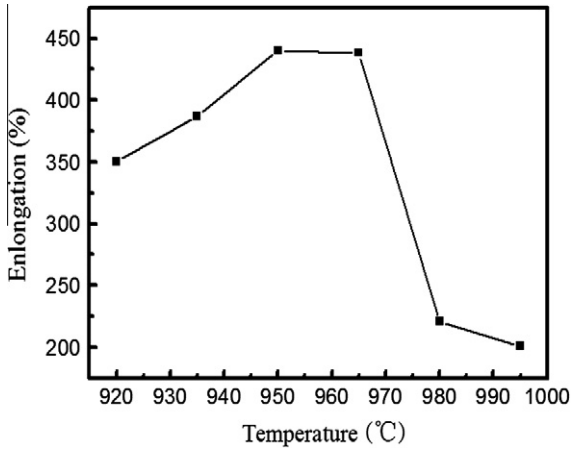

Fig. 2. Influence on elongation under different test temperature (initial strain rate $3.1 \times 10^{-4}\ s^{-1}$).

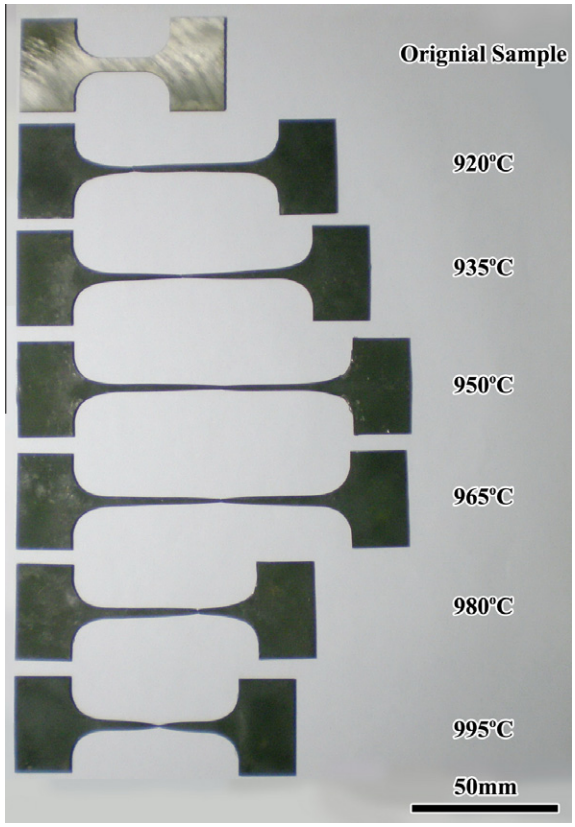

Fig. 3. Specimen after tensile test at different temperature (initial strain rate $3.1 \times 10^{-4}\ s^{-1}$).

monotone uptrend. In the initial strain rate range of the experiment, the maximum difference of initial flow stress is 35.9 MPa and the amplitude of variation is 47%. The effect of strain rate on the initial flow stress is more obvious than that of temperature.

Strain rate sensitivity value 'm' at 950 °C under different strain rate is shown in Table 2. It can be seen that when initial strain rate is changes in the $1.18 \times 10^{-4}\ s^{-1}$–$2.24 \times 10^{-3}\ s^{-1}$ at 950 °C, the alloy 'm' value increases monotonically with the decrease of strain rate. But the maximum does not exceed 0.4, the minimum is not less than 0.3 and the amplitude of variation is quite small.

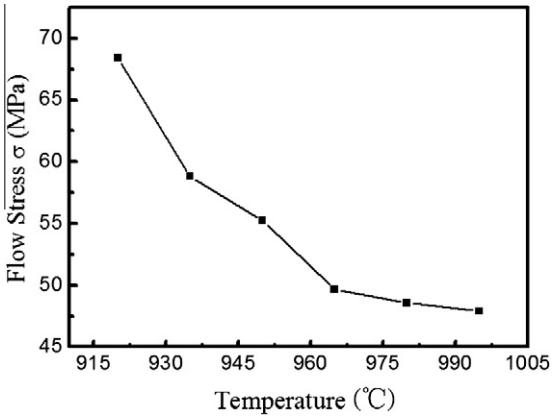

Fig. 4. Influence on initial flow stress by different test temperature (initial strain rate $3.1 \times 10^{-4}\ s^{-1}$).

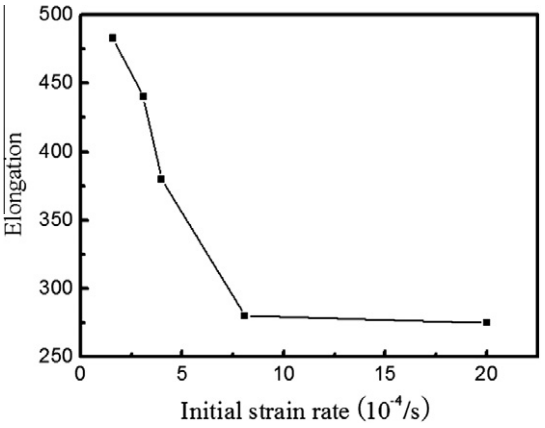

Fig. 5. Influence on elongation by different initial strain rate (test temperature at 950 °C.

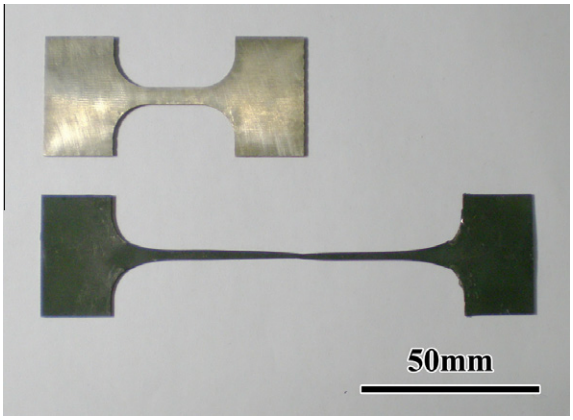

Fig. 6. Tensile specimen of Inconel718 after superplastic test at 950 °C and initial strain rate $1.6 \times 10^{-4}\ s^{-1}$ ($\Delta l/l0 = 483.6\%$).

It can be seen from the test results above, that Inconel718 superalloy with ultra-fine grain in the experiment has good superplasticity performance. The ideal superplastic forming temperature and forming rate are 950 °C and $1.6–4 \times 10^{-4}\ s^{-1}$, respectively, at which Inconel718 superalloy has greater elongation, lower flow stress and is suitable for superplastic puff forming.

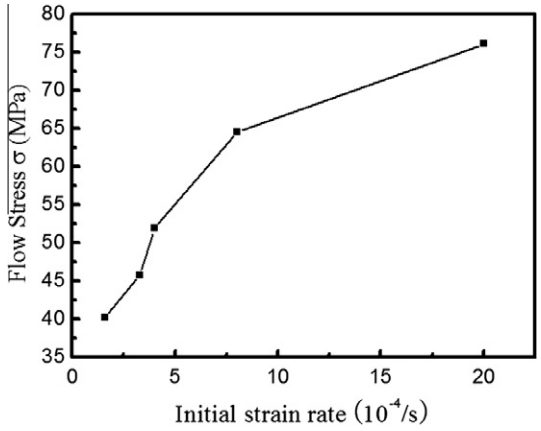

Fig. 7. Influence on flow stress by different initial strain rate (temperature at 950 °C).

Table 2
"m" Values at various initial strain rate and temperature.

Number	Deforming temperature	Initial strain rate	m
M1	950 °C	$1.18 \times 10^{-4}\ s^{-1}$	0.380
M2	950 °C	$2.08 \times 10^{-4}\ s^{-1}$	0.362
M3	950 °C	$2.56 \times 10^{-4}\ s^{-1}$	0.343
M4	950 °C	$6.20 \times 10^{-4}\ s^{-1}$	0.320
M5	950 °C	$1.56 \times 10^{-3}\ s^{-1}$	0.312
M6	950 °C	$2.24 \times 10^{-3}\ s^{-1}$	0.308

3.2. LBW/SPF technology of multi-sheet cylinder sandwich structure

3.2.1. LBW technology of multi-sheet cylinder sandwich structure

The joint forms used in the traditional welding methods are most suitable for laser welding. The laser welding joints require higher assembly precision just because the focused diameter of laser beam welding is quite small. The assembly gap of the laser butt welding joints should be less than 15% of material thickness and the roughness and dislocation is not greater than 25% [17]. The laser welding joints of multi-sheet cylinder sandwich structure mainly belong to laser penetration welding joints. In terms of the welding joint forms, it belongs to overlap joints. In terms of the overlap joint form, the assembly gap should be less than 25% of sheet thickness [17], as shown in Fig. 8. If the assembly gap of joint is too large, the above workpiece is burned through. The appropriate clamping is used in order to ensure that the relative position between workpieces does not change in the laser welding process. Therefore, the fixture should be designed to meet the assembly precision of laser welding joints of multi-sheet cylinder sandwich structure.

As the special structure of the cylindrical pieces, the laser welding fixtures should take the following questions into account: firstly, the assembly gap between the cylinders achieves the requirements in the process of laser welding of multi-sheet cylinder sandwich structure shown in Fig. 8; secondly, the fixture should be able to complete the laser butt welding of the cylinder structure; thirdly, the parts can be loaded and unloaded smoothly on the fixture in the welding process.

The variable diameter fixture will be designed to meet the assembly requirement. Through the fitting-in of the variable diameter and the external clamp, the gaps between the cylinders are reduced and eliminated. Taking the problem of loading and unloading of parts in laser welding process into account, the adjustment range of the fixture diameter is between 218 mm and 228 mm.

The key diagram of the fixture diameter variation is shown in Fig. 9. The principle of operation is as follows: when the adjustable bar forces the adjustable oblique block move axially, the adjustable oblique drives the adjuster roller to move radially due to the axial motion of the roller forbidden in the slot limit. Therefore, the changes in diameter can be achieved.

The geometry relations and the number of laser welding joint on the cylinder structure are shown in Fig. 10. So as to make superplastic forming of multi-sheet cylinder sandwich structure successful, the core cylinder can not be welded together with the inner cylinder during the welding preparation for outer cylinder and core one. Otherwise the superplastic forming of the multi-sheet cylinder sandwich structure can not be successful. In addition, the welding seam appearance should be also no welding defects such as dents, undercut. Consequently it is very important to select appropriate welding parameters to ensure that the welding request of the multi-sheet cylinder sandwich structure can be met and the welding joints have high strength as well as good weld quality and appearance at the same time. The main influence factors on the penetration of laser welding joints have output power, welding speed and defocusing amount. The defocusing amount is a fixed value of −1 mm, because it is more appropriate that the defocusing amount in the actual engineering is usually about 1 mm below the surface of the workpiece [17]. The protective gas is argon and the gas flow is 0.6 L/min. According to the relationship between the output power and penetration [18], three groups of the output power including 1000 W, 1200 W, 1400 W are selected. In terms of the relationship between the laser welding speed and penetration [18], three groups of the welding speeds involving 1000 mm/min, 1200 mm/min, 1400 mm/min are selected. Welding parameters in every group of laser welding experiment are shown in Table 3. Through the laser welding depth measurement and welding appearance, the reasonable laser penetration welding parameters are selected in these groups of the laser welding.

The joints penetrations of specimen coding L1–L9 are shown in Fig. 11a–i. By comparison in Fig. 11, the welding parameters of L1, L4, L5, L7, L8 can meet the requirements. The shear strength test results are shown on Table 4. Table 4 shows that the shear strengths increase slightly with the penetration increasing. The

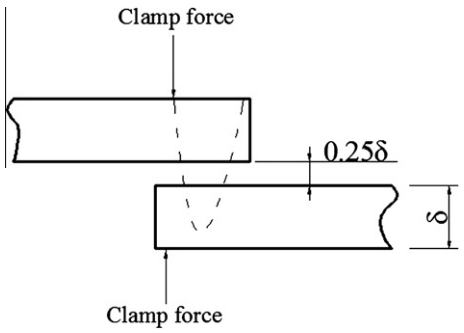

Fig. 8. Assembly precision and clamp mode of laser-welding overlap joint.

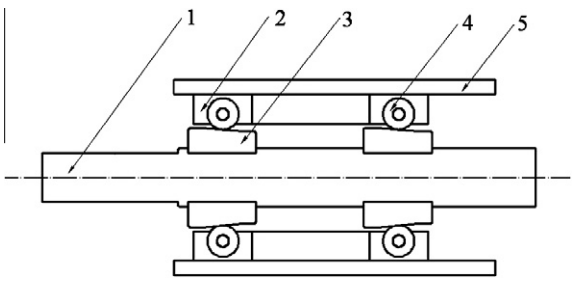

Fig. 9. The schematic diagram on the clamp of the diameter changing 1-diameter regulating stem; 2-roller wheel spacing gutter; 3-adjusting skewback; 4-adjusting roller wheel; 5-fixture internal stay.

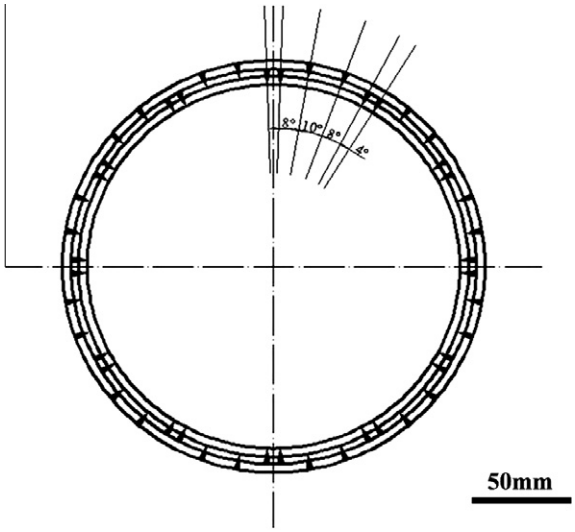

Fig. 10. Laser-welding joint geometric position relationship of the multi-sheet cylinder sandwich structure.

lowest shear strength in the experiment is 696.3 MPa, which is much higher than the joint strength of Inconel718 superalloy diffusion bonding [8]. Taking surface condition and other factors into account, L5 parameters are selected as welding parameters for multi-sheet cylinder sandwich structure. The laser butt welding parameters for the inner cylinder and the outer cylinder are: Power 900 W; Welding speed 1400 mm/min; Defocusing amount −1 mm; Shielding gas flow 0.6 L/min.

After the butt welding of the inner cylinder, the laser penetration welding between the core cylinder and the inner one is performed. After the core cylinder is stuck on the inner cylinder, the butt welding position of the core cylinder is welded on the inner cylinder according to the penetration welding parameters. With this laser welding seam on the core cylinder as the baseline, the laser scratching is carried out on the core cylinder according to Fig. 10 so that the geometric location of the other penetration welding seams is precise. After the scratching, the rest of the laser penetration welding between the core cylinder and the inner cylinder is conducted. The photo after finishing the laser penetration welding between the inner cylinder and the core cylinder is shown in Fig. 12.

Table 3
The laser-welding penetration parameters choice of multi-sheet cylinder sandwich structure.

Specimen coding	Power (W)	Welding speed (mm/min)	Defocusing amount (mm)	Shielding gas flow (MPa/min)	Joint penetration
L1	1000	1000	−1	0.1	Depth
L2	1200	1000	−1	0.1	Penetration
L3	1400	1000	−1	0.1	Penetration
L4	1000	1200	−1	0.1	Shallow
L5	1200	1200	−1	0.1	Depth
L6	1400	1200	−1	0.1	Penetration
L7	1000	1400	−1	0.1	Shallow
L8	1200	1400	−1	0.1	Depth
L9	1400	1400	−1	0.1	Penetration

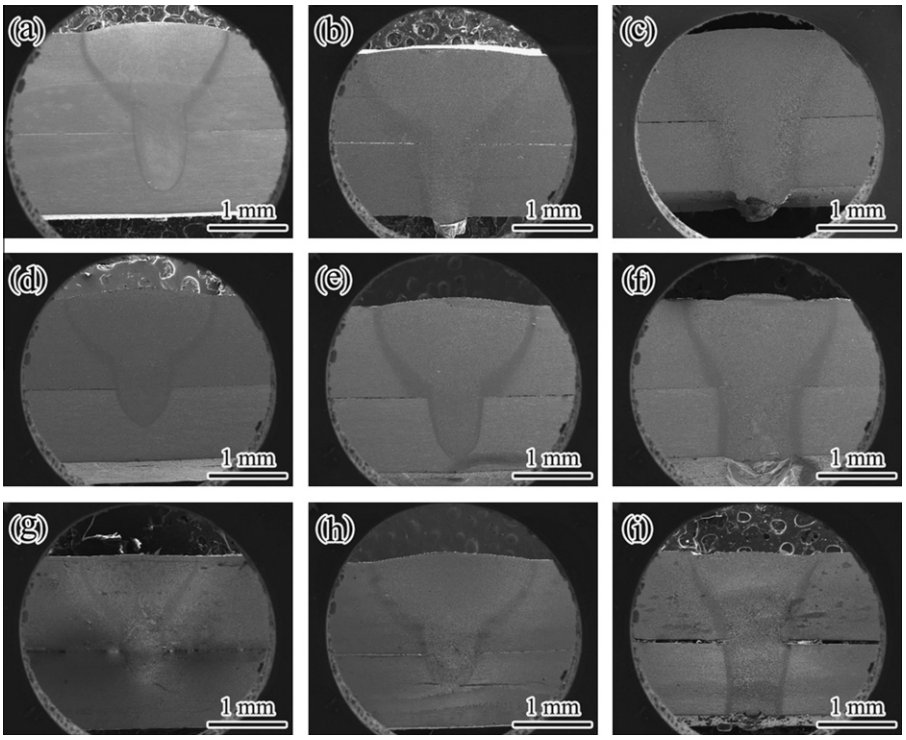

Fig. 11. The SEM photos for laser-welding penetration joint of the multi-sheet cylinder sandwich structure under the different parameters.

Table 4
The shear strength of the laser-welding penetration joints.

Specimen coding	Shear strength (MPa)
L1	712.02
L4	701.96
L5	718.50
L7	704.36
L8	696.27

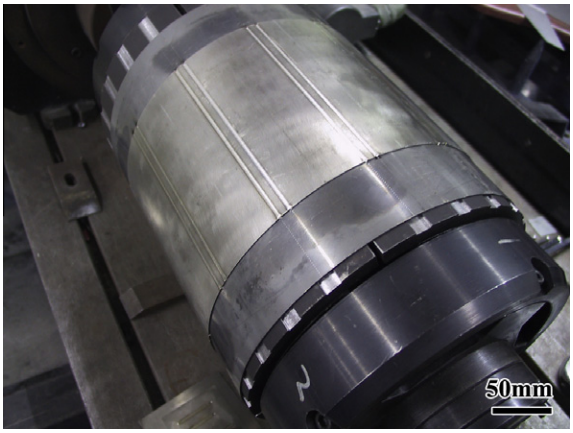

Fig. 12. The completion photo of laser penetration welding between the core and inner cylinders.

A basis line about laser penetration welding between core cylinder and outer cylinder is scratched with laser on the core cylinder according to the geometric relationship shown in Fig. 10, before the outer cylinder is loaded on the core cylinder. The outer cylinder is loaded on the core cylinder according to the baseline on the core cylinder. Because the longitudinal seam of the outer cylinder is long, a uniform laser spot welding is carried out in the laser butt welding of the outer cylinder. And then the laser scratching is proceeding on the outer cylinder as the baseline with the laser butt welding seam according to Fig. 10. The laser penetration welding of the outer cylinder is performed after the laser scratching. After all the laser penetration welds are completed, the longitudinal seam welding is finalized. The workpieces photo after finishing the laser penetration welding is shown in Fig. 13.

3.2.2. SPF technology of multi-sheet cylinder sandwich structure

Higher demands are presented to the SPF die material because of the complexity of multi-sheet core cylinder structure. The die material should have the following properties: good mechanical properties in high temperature; good performance in rapid thermal and quench; good oxidation resistance in high temperature; good machining properties; high phase transition temperature. In consideration of these factors, heat resisting cast-steel 35Cr24NiSiNRe is used in the experiment. The mechanical properties of the material are shown in Table 5. The superplastic forming die scheme of multi-sheet cylinder sandwich structure is shown in Fig. 14.

The superplastic parameters for the multi-sheet cylinder sandwich structure include forming temperature, the rate of loading pressure in forming, the final pressure, dwell time. The selection criteria are as follows:

(1) The temperature in SPF process.

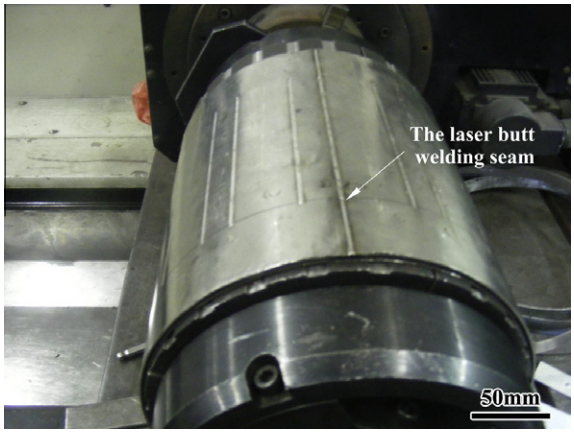

Fig. 13. The cylinder piece photo after the completion of laser penetration welding and butt welding.

The low flow stress and the large elongation are required in superplastic forming of multi-sheet cylinder sandwich structure. And at the same time a higher forming temperature is chosen in favor of transformation and dissolution of Laves phase produced in the laser welding process. From the experimental results of Section 3.1, forming temperature is selected at 950 °C.

(2) The rate of loading pressure, final pressure and dwell time in SPF process.

The action of pressure is to ensure no welded position to form smoothly. The internal structure of Inconel718 superalloy multi-sheet cylinder sandwich structure is complex. In order to ensure the structure to form successfully, the slow rate of loading pressure, the higher final forming pressure and the long dwell time should be selected. The relationship curve between the pressure and time is shown in Fig. 15.

The photo of the multi-sheet cylinder sandwich structure after superplastic forming is shown in Fig. 16. It can be seen in Fig. 16 that multi-sheet cylinder sandwich structure after SPF has high symmetry of internal structure, the full formed outer wall, no dents and other defects. This result is indicating that the selection of the parameters of SPF process is correct. The forming experiment result shows that LBW/SPF technology is suitable for manufacturing multi-sheet cylinder sandwich structure of Inconel718 superalloy.

3.3. Microstructures and mechanical properties of multi-sheet cylinder sandwich structure

3.3.1. Microstructures and mechanical of laser welding joint

Microstructures in the weld fusion are shown in Fig. 17a and b. From Fig. 17. It is noted the dendritics occurred in the weld fusion. The dendritics in the weld fusion zone are observed to be fine and equiaxed in the weld interior and to be slightly coarser and columnar at region adjacent to the fusion boundary. The phenomenon observed to be very fine and equiaxed in the weld interior and to be slightly coarser and columnar at regions adjacent to the fusion boundary can be explained with the basis of thermal gradient (G) and cooling rate or growth rate (R). According to the theory of morphological stability originally developed by Mullins and Sekerka [19], the temperature gradient (G) and the growth rate (R) are very important in the combined form G/R or GR as they influence the solidification morphological: Plan → Cell → Dendrites and the dimension of solidification structure. It is well known that the degree of undercooling in a solidifying melt is inversely proportional to the ratio of thermal gradient to growth rate (G/R). Thermal

Table 5
Mechanical properties of die materials in the experiment.

Material	Room temperature			High temperature		
	σ_b (MPa)	δ (%)	ψ (%)	σ_b (MPa)	δ (%)	ψ (%)
35Cr24Ni7SiNRe	770–820	20–40	16–40	1000 °C, 53–88	1000°C, 28–67	29–58

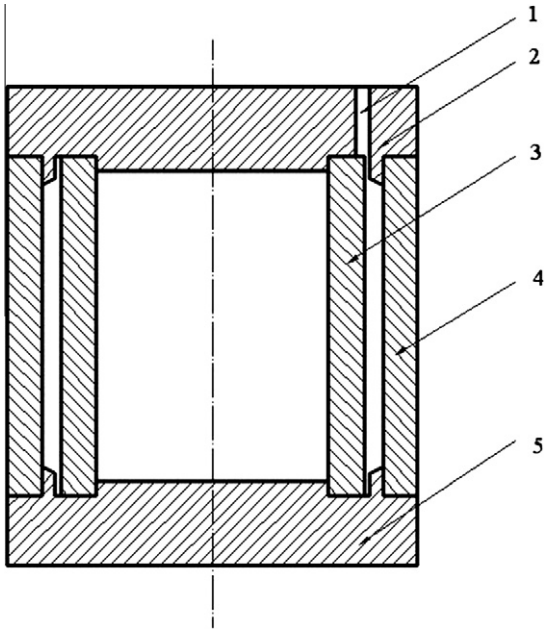

Fig. 14. The die for SPF of multi-sheet cylinder sandwich structure of Inconel718 superalloy 1-admitting pipe passage in bulging time; 2-die head cap; 3-die inner core; 4-die outer canister; 5-die lower cover.

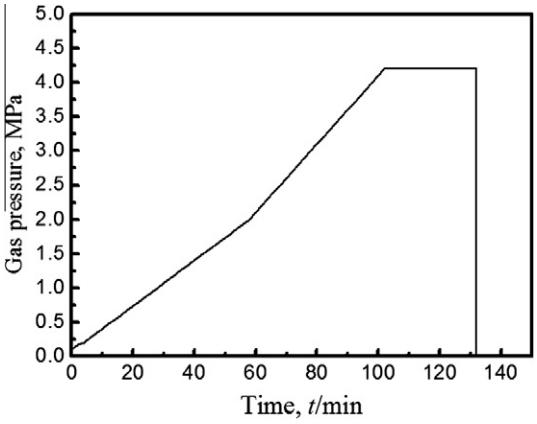

Fig. 15. The relationship between the gas pressure and time for multi-sheet cylinder sandwich structure.

gradients in a weld pool are steeper at regions close to fusion boundary than in weld interior [20]. The steeper thermal gradients prevailing at the fusion boundary is responsible for columnar dendritic growth in a direction opposite to the heat extraction direction. Towards the weld center, however, the thermal gradients are not as steep, which in combination with the very rapid cooling rates characteristic of laser beam welding, results in significant undercooling (low G/R) leading to the formation of fine equiaxed dendrites.

It is interesting to note the welds are found to be free from HAZ microfissuring in Fig. 17b. This is mainly contributed to the grain size which has a great influence on microfissuring: finer grain size

Fig. 16. The photo of the whole multi-sheet cylinder sandwich structure after SPF process.

is less prone to microfissuring and vice versa [21]. Usually, the grain level of ASTM10 [15] in base material can avoid the appearance of microfissuring in HAZ. In the present study, laser beam welding was carried out in Inconel718 superalloy with ultra-fine grains (ASTM13-14 [15]). Therefore, this effectively inhibits the production of HAZ microfissuring. The HAZ in the experiment is observed to be narrow with slight grain growth in HAZ compared to the base material because of the very low heat input in the LBW process.

The SEM microstructures of the weld fusion zone are shown in Fig. 18a (at weld center) and b (adjacent to fusion boundary). As can be seen, an amount of precipitated phases (bright phases) occurred in the weld fusion zone. The distribution state of precipitated phase in the weld center is different from that adjacent to the fusion boundary. The precipitated phases in the weld center distributes discretely. But distribution of precipitated phases adjacent to the fusion boundary is slightly regular and directional. The characteristic of distribution of precipitated phase is related to optical morphology seen in these regions. Fig. 19 shows the results of EDAX spectrums on precipitated phase and dendritic core. Using the EDAX spectrum, it is founded that the element fraction of the dendrites is different from that of the precipitated phase in the interdendritics. The average element contents of dendritic core and precipitated phase are shown in Table 6. Through Table 6, it is found that the precipitated phase is rich in Nb, Mo, Ti and lean in Ni, Cr, Fe compared to the base material. But dendritic core is lean in Nb, Ti, Al. The element fraction characteristic shows that the precipitated phase is Laves phase which presents in the cast and welded products of Inconel718 superalloy.

The difference of element fraction in the dendritic core and the precipitated phase indicates that there is ingredient segregation in the solidification process of LBW. Inconel718 superalloy is precipitation strengthened primarily by γ'' which is based on composition Ni_3Nb. The sluggish aging kinetics of γ'' precipitation is also found to be beneficial to material's weldability [22]. However, as niobium is a high concentration refractory element, it tends to segregate during the solidification process, as a result of the fact that some desirable phase, like Laves phase, can form in the welding fusion. Laves phase is a hexagonally close packed phase and generally

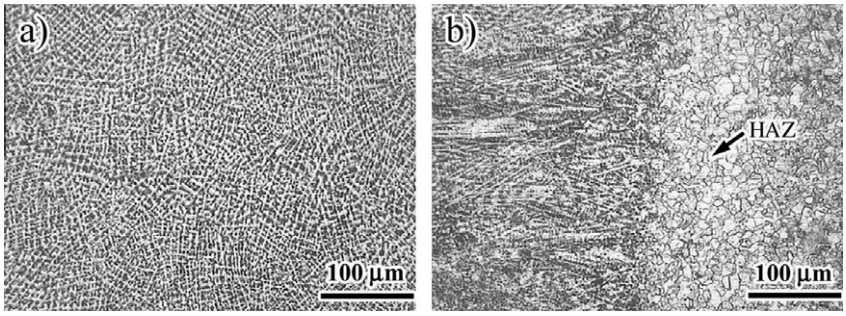

Fig. 17. Microstructure of fusion zone (as-welded condition): (a) microstructure showing very fine equiaxed dendrites in the weld interior; (b) microstructure showing columnar dendrites adjacent to the fusion boundary (arrow shows heat affected zone).

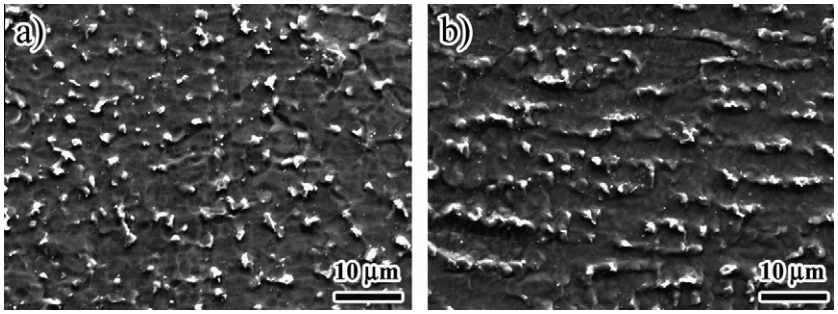

Fig. 18. Microstructure of fusion zone (as-welded condition): (a) microstructure in the weld interior showing fine discrete Laves particles; (b) microstructure showing a certain ordination Laves particles adjacent to the fusion boundary.

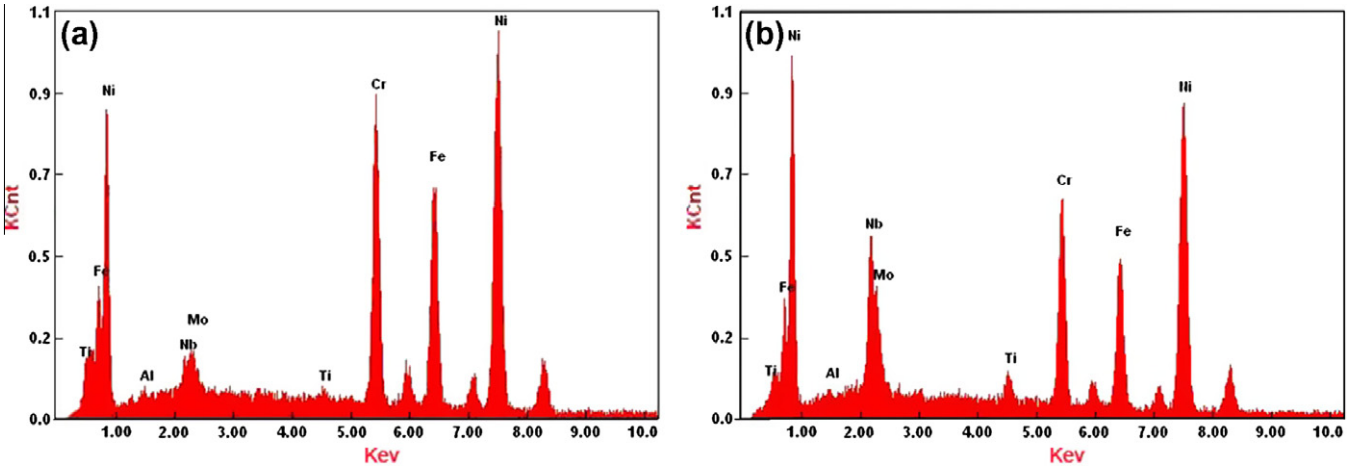

Fig. 19. EDAX spectra of weld joint obtained (a) dendritics; (b) precipitated phase.

Table 6
Elements content of dendritic and precipitated phase in weld joint.

	Ni	Fe	Cr	Nb	Mo	Ti	Al
Dendritic	54.63	19.16	19.51	2.82	2.72	0.65	0.51
Precipitated phase	48.55	14.39	16.40	14.58	3.82	1.49	0.78

accepted [23] to be of the form $(Ni, Fe, Cr)_2$ (Nb, Mo, Ti). Because of this unique chemical composition of Laves phase, as mentioned above, it can be distinguished from the other phases existing in Inconel718 superalloy. The formation of Laves phase requires a niobium concentration ranging from 10% to 30%. The occurrence of Laves phase is a serious problem to Inconel718 superalloy because Laves phase will deplete the key alloy element Nb, the mainly strengthening element in Inconel718 superalloy, and result in the composition inhomogeneity in the alloy. Furthermore, Laves phase in Inconel718 superalloy is detrimental to weld mechanical properties, particularly to tensile ductility, fracture toughness fatigue and propagation. Therefore, Laves phase in the weld fusion should be eliminated in order to ensure regular service of the multi-sheet cylinder sandwich structure.

As shown in Fig. 20a (in the weld interior) and b (adjacent to the fusion boundary), both the equiaxial dendritics in the weld interior and the columnar dendrities adjacent to the fusion boundary became coarser after SPF process. The phenomenon that the dendritics in the weld fusion grew slightly after SPF process is mainly because the weld fusion zone was exposed in the thermal cycle generated by SPF process. Because of the same reason, the grains in the HAZ grow slightly.

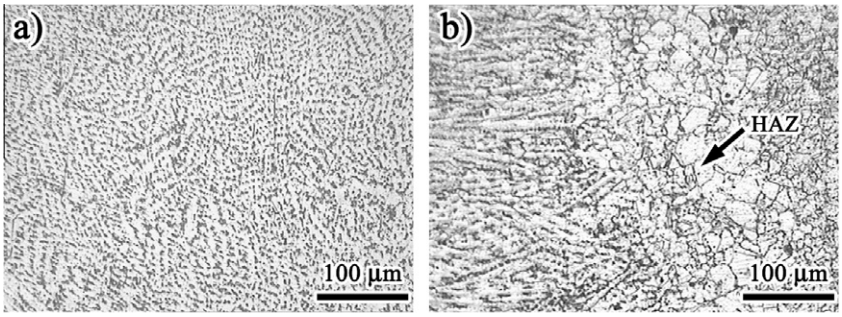

Fig. 20. Microstructure of fusion zone after SPF process: (a) Fusion zone microstructure in the weld interior; (b) Fusion zone microstructure adjacent to the fusion boundary.

The SEM microstructures of the weld fusion in post-SPF condition are shown in Fig. 21a (in the weld interior) and b (adjacent to the fusion boundary). Many needle-like precipitated phases occur in the post-SPF weld fusion but a small amount of globosity precipitated phase still preserve. Fig. 22 shows the EDAX result of needle-like, globosity precipitated phase and dendritics. Table 7 shows the fraction of the precipitated phase and dendrities. From the result of EDAX spectrum, the segregation of Nb element in the weld fusion has been improved after SPF process. Nb concentration of the post-SPF dendritics in the weld fusion has been increased to 5.42%. Most of Laves phase dissolves after SPF process. Nb concentration of needle-like precipitated phase in the weld fusion after SPF process is about 8.03%. From the results of EDAX, the precipitation is δ precipitated phase. The δ-phase in Inconel718 superalloy is an equilibrium Ni_3Nb with orthorhombic crystal structure which requires about 6–8% Nb element and precipitates in the range of 860–995 °C [18]. In the weld metal solidification, the interdendritic regions become enriched in Nb with concentration in the range of 6–10% or more, and Nb concentration in regions where Laves particles form is more than 10%. Thus, at the end of solidification, there will be the regions around Laves phase in the weld metal with sufficient Nb concentration where δ precipitated phase can form. However, rapid cooling rates through the δ-phase precipitation range during weld metal preclude δ-precipitation in these regions. Because SPF temperature of multi-sheet cylinder sandwich structure is in the δ precipitation range, as in the present case at 950 °C, δ-phase precipitation occurs in these regions and results in moderating Nb concentration around the Laves particles. Further, because of the Laves dissolution occurring simultaneously during the SPF process of multi-sheet cylinder sandwich structure, some amount of Nb gets released into surroundings and this results in making available more Nb for δ-phase precipitation. Otherwise, the SPF process of the multi-sheet cylinder sandwich structure proceeded under 950 °C and forming time was as long as 130 min. The long forming time and the high deformed temperature make for Nb's diffusion to the dendritics in the weld metal. Nb which diffused into the dendritics in the weld fusion comes partly from that released by Laves phase dissolution and partly from that originally rich in the interdendritics. So Nb's distribution homogeneity in the weld metal results in that Nb concentration in the dendritics increased obviously after SPF process. But in the weld fusion, there has been still undissolved Laves phase after SPF process. This is attributed to the fact that whether Laves phase can be dissolved easily or difficultly depends on its Nb concentration and size. Coarser Laves particles with higher Nb concentration require higher temperature and soak time for dissolution. Consequently, some Laves phases are reserved after SPF process because of its bigger dimension and higher Nb concentration. In this paper, niobium segregation can be resolved in a certain extent after SPF process. The hardness test results in the weld fusion show that the post-SPF hardness increased up to 391.74 HV compared to 331.63 HV in as-weld condition which is closed to the base material hardness of 415.63 HV in post-SPF condition. These results show that LBW/SPF is an appropriate composite technology for the manufacture of multi-sheet cylinder sandwich structure of Inconel718 superalloy.

3.3.2. Microstructure and the mechanical properties of the base material

The microstructure of post-SPF base material of multi-sheet cylinder sandwich structure is shown in Fig. 23. And there was slight growth of grain size compared to as-received condition. But the grain size of post-SPF base material still maintained as small as less than 10 μm and there were no cavities in post-SPF base material. This is contributed to the less deformation of base material in SPF process. Besides, because SPF temperature is in the temperature range of δ-phase precipitation, many δ precipitated phases in SPF process are also helpful to control the grain size, as shown in Fig. 23. Table 8 shows the result of base material tensile properties in as-received and post-SPF condition. Tensile strength of post-SPF goes up compared to the as-received and ductility decrease. The hardness of base material ascends to 415.63 HV compared to

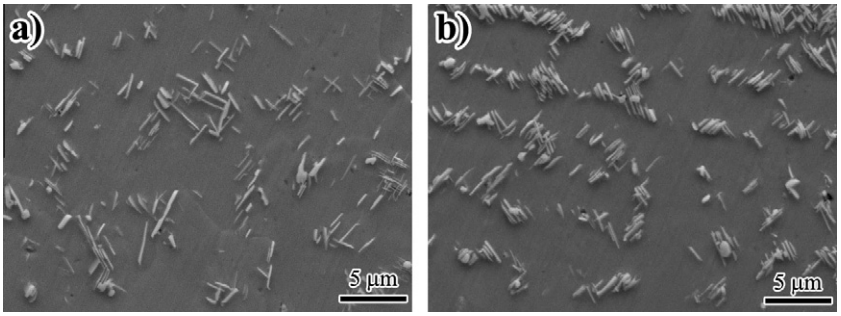

Fig. 21. SEM microstructure of the weld fusion zone after SPF (a) microstructure in the weld interior; (b) microstructure adjacent to the fusion boundary.

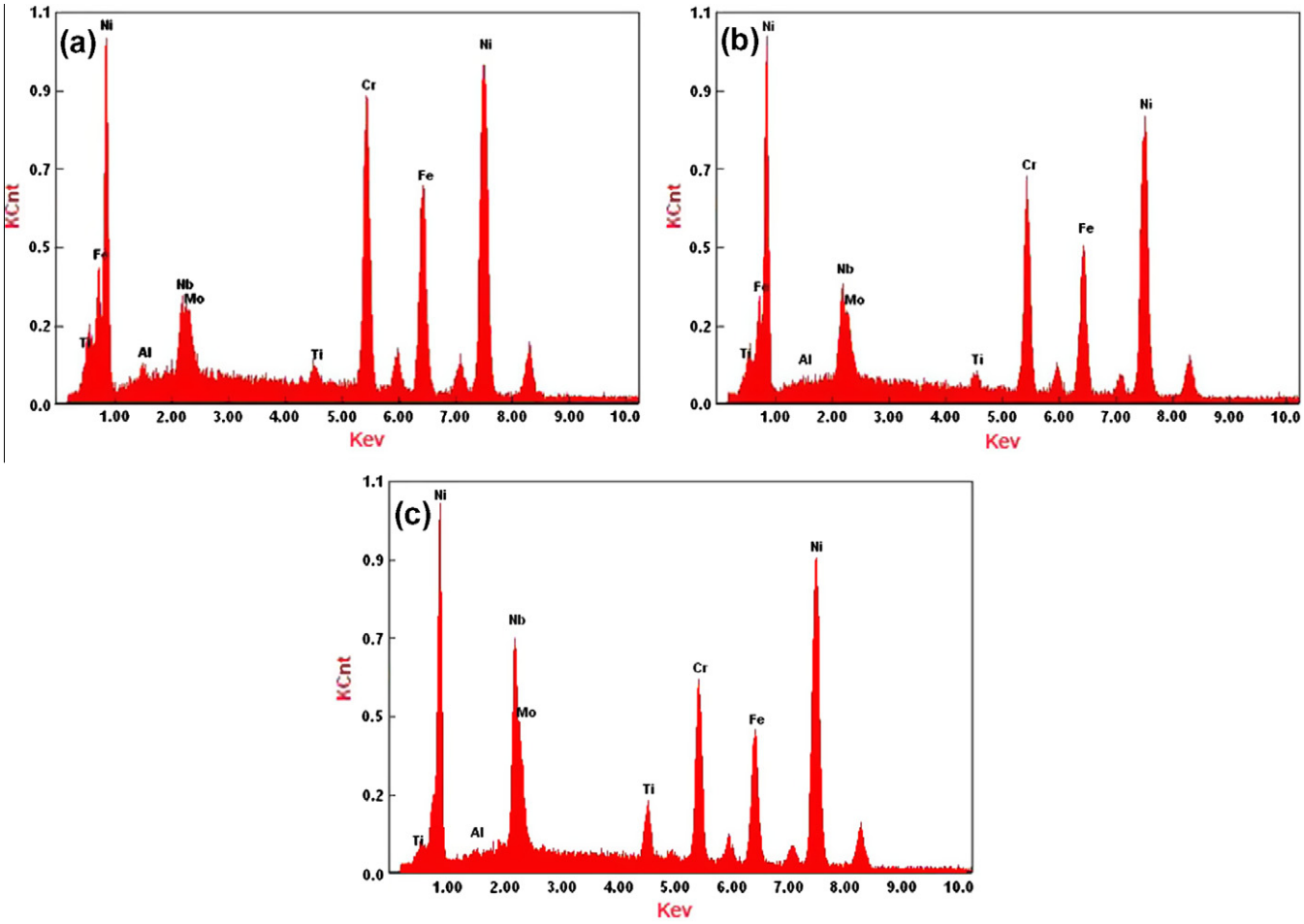

Fig. 22. EDAX spectra obtained after superplastic forming (a) dendritcs; (b) acicular precipitated phase; (c) spherical precipitated phase.

Table 7
Elements content of dendritic and precipitated phase after superplastic forming (mass fraction (%)).

	Ni	Fe	Cr	Nb	Mo	Ti	Al
Dendritic	53.04	18.24	18.06	5.42	3.42	1.11	0.6
Needle-like precipitated phase	52.23	16.94	17.01	8.03	2.84	1.48	0.49
Spheric precipitated phase	47.51	15.86	15.63	14.73	3.94	1.67	0.66

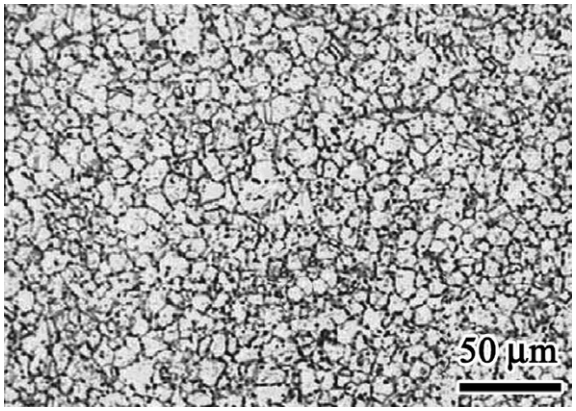

Fig. 23. Microstructure of base material under post superplastic forming.

390.28 HV in as-received condition. By the tensile result of the base material, it is well known that these precipitated phases were not only δ precipitated phase but also γ'' and γ'' phase, because δ-phase is incoherent with the matrix and contributes very little to base material hardness and strength.

Table 8
Room temperature tensile test results.

Condition	σ_b (MPa)	$\sigma_{0.2}$ (MPa)	δ (%)
As-received	1061	587.8	47.283
Post-SPF	1284	888.2	33.343

4. Conclusion

The goal of this study is to identify whether multi-sheet cylinder sandwich structure can be manufactured by LBW/SPF technology or not. Through systematic experiments, the experiment results show that LBW/SPF technology can fabricate multi-sheet cylinder sandwich structure. Results of this experimental study can be summarized as follows:

(1) When Inconel718 superalloy with ultra-fine grain deforms at a temperature of 920–995 °C with initial strain rate of $3.1 \times 10^{-4}\ s^{-1}$, the elongation percentage is between 200% and 440%. The elongation increases as the temperature increasing at 920–950 °C. But when the deforming temperature reaches or exceed 980 °C, the elongation of percentage of the sheet decreased significantly. At a temperature of 950 °C with a strain rate of $1.6 \times 10^{-4}\ s^{-1}$–$2.0 \times 10^{-3}\ s^{-1}$, the elongation of the sheet changes between 275% and 483.6%. At 950 °C with a strain rate of $1.6 \times 10^{-4}\ s^{-1}$, the elongation rate is 483.6%. When initial strain rate is changed in the $1.18 \times 10^{-4}\ s^{-1}$–$2.24 \times 10^{-3}\ s^{-1}$ and the temperature is changed at 950 °C, the alloy 'm' value is between 0.3 and 0.4. The appropriate superplastic forming temperature for Inconel718 superalloy with ultra-fine grain is at 950 °C;

(2) The welding fixture for multi-sheet cylinder sandwich structure is designed. The welding problem of the multi-sheet cylinder sandwich structure is solved by changing the diameter of the fixtures. The reasonable laser penetration welding parameters of the multi-sheet cylinder sandwich structure are: power 1200 W, welding speed 1200 mm/min, defocus amount of −1 mm, shielding gas flow 0.6 L/min; the laser butt welding parameters are: power 900 W, welding speed 1400 mm/min, defocus amount −1 mm, shielding gas flow 0.6 L/min. The parameters for superplastic forming are as follows: temperature $T_f = 950$ °C, pressure $P_f = 4.2$ MPa, time $t_f = 130$ min. The multi-sheet cylinder sandwich structure by LBW/SPF composite technology has good shape, uniform wall thickness distribution, the high symmetry of internal structure.

(3) The microstructures in as-weld and post-SPF condition are investigated. Laves phase and Nb segregation occur in interdendritics of the weld fusion zone. Nb concentration in dendritics is relatively low compared to the base material. After post-SPF process, most Laves precipitated phases turn into δ precipitated phase and Nb concentration in the dendritics is improved greatly. The hardness in the weld fusion increases obviously after SPF process. The grain size of base metal after superplastic forming grows up in by a certain degree. But because the forming temperature is in the range of δ phase precipitation and the deformation is smaller, the grain in the base metal grows substantially slightly. The yield strength of the base material increases.

References

[1] Gobbi S, Zhang Li, Norris J, Richter Kh, Loreau JH. High power CO_2 and Nd-YAG laser welding of wrought Inconel 718. J Mater Process Technol 1996;56:333.

[2] Nalbant Muammer, Altın Abdullah, Gökkaya Hasan. The effect of coating material and geometry of cutting tool and cutting speed on machinability properties of Inconel 718 super alloys. Mater Des 2007;28(5):1719–20.

[3] Chiozzi S, Dattoma V, Panella F. Capacitor discharge welded bars of Inconel 718 and TiAl6V4 superalloys under fatigue. Mater Des 2008;29(4):839–40.

[4] Thakur DG, Ramamoorthy B, Vijayaraghavan L. Study on the machinability characteristics of superalloy Inconel 718 during high speed turning. Mater Des 2009;30(5):1718–9.

[5] Smith Gaylord D, Lee Flower H. Superplastic Forming of Alloy 718. Mater Processes 1994;4:32–4.

[6] Yeh MS, Chuang TH. Superplastic forming/brazing process for Inconel 718 superalloy components. Weld Res Sup 1997:197–200.

[7] Xue Han, Hui Xia, et al. The extrusion processing for superalloy GH4169. Metal Form Technol 1997;15(15):24–6.

[8] Wen-bo Han, kai-feng Zhang, et al. Research on microstructures and properties of diffusion bonding joints for Inconel 718 superalloy. Mater Sci Technol 2005;3(13):308–11.

[9] Dong JX, Xie XS, Zhang SH. Coarsening behavior of γ'' precipitates in modified Inconel 718 superalloy. Scripta Mater 1995;33(12):1933–9.

[10] Ram GDJ, Reddy AV, Rao KP, Reddy GM. Control of laves phase in Inconel 718 GTA welds with current pulsing. Sci Technol Weld Join 2004;9(5):390–8.

[11] Gregori A. A survey of welding and repairing of nickel superalloys for gas turbines. TWI, Report No. 774; 2003.

[12] Ram GDJ, Reddy AV, Rao KP, Reddy GM, Sundar JKS. Microstructure and tensile properties of Inconel 718 pulsed Nd–YAG laser welds. J Mater Process Technol 2005;167(1):73–82.

[13] Cam G, Kocak M. Progress in joining of advanced materials. Int Mater Rev 1998;43(1):1–44.

[14] Li ZQ, Li XH. The application of SPF/DB combined with welding technologies. Mater Sci Forum 2007;551–552:49–54.

[15] ASTM E 112–1996. Standard test methods for determining average grain size. ASTM International, West Conshohocken, Pennsylvania, United States; Published in November 2004.

[16] CHINA AERONAUTICAL MATERIALS HANDBOOK. Editorial Board, CHINA AERONAUTICAL MATERIALS HANDBOOK. Beijing: Standards Press of China; 2002.

[17] Zhang KK, Xue YM. Special advanced connection method. Haerbin: Harbin Institute of Technology Press; 2008.

[18] Li ZY, Qian YY, Zhang JH. Advanced connection method. Beijing: Machinery Industry Press; 2000.

[19] Mullins WW, Sekerka RF. Stability of a planar interface during solidification of a dilute binary alloy. Journal of Applied Physics 1964;35(2):444–51.

[20] David SA, Vitek JM. Principles of weld metal solidification and microstructures. In: David SA, Vitek JM. editors. Conference proceedings on trends in welding research. Gatlinburg, TN, USA; June 1–5 1992. p. 147.

[21] Thompson RG et al. The relationship between grain size and microfissuring in alloy 718. Weld J 1985;4:91S–6S.

[22] Radavich JF. The physical metallurgy of cast and wrought alloy 718. In: Loria EA, editor. Conference Proceedings on Superalloy 718-Metallutgy and Applications. The Minerals, Metals & Materials Society; 1989. p. 229.

[23] Schirra JJ, Caless RH, Hatala RW. In: Loria EA, editor. Superalloy 718, 625 and various derivatives. Warrendale, PA: TMS; 1991. p. 375–88.